Volume 1 | Number 1 | Jan 2013 | Pages 1–100

Journal of
Materials Chemistry B

Materials for biology and medicine
www.rsc.org/materialsB

ROYAL SOCIETY
OF CHEMISTRY

This is an *Accepted Manuscript*, which has been through the Royal Society of Chemistry peer review process and has been accepted for publication.

Accepted Manuscripts are published online shortly after acceptance, before technical editing, formatting and proof reading. Using this free service, authors can make their results available to the community, in citable form, before we publish the edited article. We will replace this *Accepted Manuscript* with the edited and formatted *Advance Article* as soon as it is available.

You can find more information about *Accepted Manuscripts* in the **Information for Authors**.

Please note that technical editing may introduce minor changes to the text and/or graphics, which may alter content. The journal's standard **Terms & Conditions** and the **Ethical guidelines** still apply. In no event shall the Royal Society of Chemistry be held responsible for any errors or omissions in this *Accepted Manuscript* or any consequences arising from the use of any information it contains.

ARTICLE

Hydroxyapatite-Fe₂O₃ based material of natural origin as an active sunscreen filter

C. Piccirillo,[a]* C. Rocha,[ab] D.M. Tobaldi,[c] R.C. Pullar,[c] J.A. Labrincha,[c] M.O. Ferreira,[d] P.M.L. Castro,[a] and M.M.E. Pintado[a]

The use of sunscreens as a protective barrier against skin damage and cancer, by absorbing harmful UVA and UVB rays, is becoming an increasingly important issue. Such products are usually based on TiO_2 or ZnO, although both Fe_2O_3 and hydroxyapatite ($Ca_{10}(PO_4)_6(OH)_2$, HAp) doped with metal ions have been reported as being ultraviolet (UV) absorbing materials. HAp is the main component of bone; it is, therefore, highly biocompatible. In the present work, an iron-doped HAp-based material, containing both Fe ions substituted into the HAp structure and iron oxide in hematite (α-Fe_2O_3) form, was successfully developed from waste cod fish bones. This was achieved through a simple process of treating the bones in a Fe (II) containing solution, followed by heating at 700 °C. The material showed good absorption in the whole UV range and did not form radicals when irradiated. Sun cream formulated with this material could be used as a broad sunscreen protector ($\lambda_{crit} > 370$ nm), showing high absorption both in the UVA and UVB ranges. Because of its absorption properties it would be classified as 5 star protection according to the Boots UVA star rating system. The cream is also photostable, and does not cause irritation or erythema formation when in contact with human skin. These results show that a food by-product such as fish bones could be converted into a valuable product, with potential in health care and cosmetics. This is the first time a HAp-based sunscreen cream has been developed and validated as proof of concept.

Introduction

It is well known and accepted that exposure to ultraviolet (UV) light from the sun can cause extensive damage to the skin, such as erythema and sun burn. Moreover, long term health effects, in particular skin cancer, can also be developed.[1,2] The UV spectrum is divided into three regions, according to the wavelength of the light: UVC (200-290 nm), UVB (290-320 nm) and UVA (320-400 nm). UVC radiation is mainly blocked by the ozone layer in the upper atmosphere, while UVB and UVA are not; they can, therefore, pose a threat to human health. The UV sunlight at the Earth's surface is approximately 98% UVA and 2% UVB, and while UVB is responsible for the most severe damage to DNA and RNA, UVA has important roles in photoaging and photocarcinogenesis.[3] Both forms of UV light interact with the human body through both direct photochemistry and the formation of secondary radicals and reactive oxygen species.[4]

The use of sunscreens is one of the most common and effective ways to prevent the damage associated to UVA and UVB

radiations. Ideally, a sunscreen product should protect the skin in both the UVA and UVB regions to fully prevent the ascribed health problems.[4] Moreover, a sunscreen should be stable over time, and not degrade under irradiation. It is also important that the chemicals the sunscreen is made of are non-toxic for human health, do not cause irritation to the skin, and do not penetrate in the skin itself.[1]

Titanium dioxide (TiO_2) and zinc oxide (ZnO) are the most common inorganic materials used in commercial sunscreens: both compounds provide protection over the whole UV range.[5] Literature data show that using these compounds in the form of nanoparticles improves their effectiveness, leading to an enhanced protection.[6] At the same time, however, there is concern about the possible toxicity of the nanoparticles; although several studies were published on the subject, to date there is no incontestable evidence on this topic.[7,8] For TiO_2 and ZnO use, however, another possible risk is associated with their photocatalytic properties under UV and visible light. Both minerals are in fact photochemically reactive compounds; this means that, under irradiation, they can form free radicals and other reactive species that can cause some of the health problems associated with

UV exposure. Scientific studies, for instance, showed that the formation of radical species can occur for ZnO-containing sunscreens under illumination,[9] and such reactive species could potentially be as dangerous for the skin as much as the UV light itself. Small TiO_2 particles have also been shown to have serious effects on mitochondrial function, altering 85 biochemical metabolites, many of which are associated with the cellular stress response.[10] Moreover, due to the great increase in sunscreen use in recent years, some of the active components have been detected in increasing concentrations in the environment proving adverse effects. Indeed, significant concentrations of both TiO_2 and ZnO have been found in coastal waters.[11]

Iron oxide in its hematite form (α-Fe_2O_3) is an inorganic compound which is often added to sunscreen creams due to its reddish colour.[1,12] Recently, however, its potential as a UV absorber has been also considered. Truffault,[13] for instance, showed that water-oil emulsions containing hematite nanoparticles can provide effective sun protection for both UVA and UVB ranges.

Hydroxyapatite ($Ca_{10}(PO_4)_6(OH)_2$, HAp) is a calcium phosphate compound, highly present in nature. It is a non-toxic material, being the main component of human and animal bones; it has a high biocompatibility; because of this, HAp is used to make bone and dental implants.[14] Because of its non-toxicity, it would be a very suitable material as base for sunscreen filters. Unmodified HAp, however, does not absorb in the UV range, so it is necessary to modify its structure to obtain a UV-absorbing material. Doping with appropriate elements may provide final compounds with promising UV protection. Studies performed by Araujo *et al.* show that zinc, iron or manganese doping can affect the HAp UV absorbing spectrum; manganese and iron, in particular, were the most effective metals.[15,16] HAp was also studied as a possible UV protection agent in a polyester matrix.[17]

The majority of HAp used today is synthetic. Several methods have been reported for its preparation, which are normally based on a reaction between calcium- and phosphorus-containing compounds. However, HAp can also be obtained from natural sources in particular from waste by-products with several environmental benefits; in a previous study carried out by the authors of the present study, HAp-based materials were extracted from cod fish bones (a waste by-product of the fish industry) as a valorisation product. The results showed that both single-phase HAp, and a bi-phasic material made of HAp and β-tricalcium phosphate (β-TCP), can be obtained by simply calcining the bones.[18] Moreover, it was also shown that the composition of the material can be changed with a simple pre-treatment of the bones in an appropriate solution; in some cases, this led to the introduction of specific ions in the HAp lattice. In other cases, however, a multiphasic material was obtained; treating the bones with a Ti-containing solution, for instance, led to a HAp-TCP-TiO_2 material with excellent photocatalytic properties.[19]

In this paper, we report the study on a HAp-based multiphasic material with UV-absorbing properties and, hence, showing potential as a sunscreen. The material was obtained from the cod fish bones using the same principles applied before - that is by modifying them with a suitable treatment in solution. In this case, the bones were treated in a Fe (II) solution and successively calcined; iron was chosen considering

the previous published results [15] and because it is, potentially, less toxic than manganese. The product was a multiphasic material containing, HAp, Fe-substituted HAp and a small amount of hematite, and it absorbed radiation over the whole UV range, without releasing any radical species under irradiation. Considering these properties, this sample was tested as an additive in a cream to explore its potential as sunscreen cream. To the best of our knowledge, this is the first time that a HAp-based sunscreen cream has been formulated. The UV protection efficacy and the photostability of the cream were assessed; moreover, a test to determine the dermatological sensitivity to the cream was also performed.

Experimental

Powder preparation

Cod fish bones (from Pascoal & Filhos) were washed and stored at -20 °C. Prior to use, they were defrosted and dried at 45 °C overnight.

To prepare the samples, a weighed amount of bones was placed in an iron (II) chloride ($FeCl_2$) solution. $FeCl_2$ concentration was 5 times higher than the HAp concentration, calculated assuming a 70% HAp content in the fish bones. The pH of the solution, initially acidic (2.9 – 3), was adjusted to 8.0 with the addition of 1M NH_4OH solution.

The bones were left stirring in this solution for 3 hours, at 65-70 °C. The bones were then dried at 45 °C overnight, and then calcined at 700 °C; the heating/cooling rate was 5 °C/min, while the calcining time was 1 hour.

Powder characterisation

To establish the elemental composition of the sample, the concentration of calcium, phosphorus and iron were measured. A weighed amount of sample was dissolved in a HNO_3 solution, which was then used to determine the concentration of each element. For calcium, flame atomic absorption spectroscopy (FA-AAS) was used, with a UNICAM 960® spectrophotometer (Waltham, USA). Phosphorus was determined by a spectrophotometric method: the solution was reacted with the Merck Spectroquant phosphorus reagent kit, containing an acidified solution of NH_4VO_3 and $(NH_4)_6Mo_7O_{24} \cdot 4H_2O$ to form an orange-yellow coloured compound of $H_4PMo_{11}VO_{40}$ (molybdovanadophosphoric acid). This compound was analysed spectrophotometrically, using a Perkin Elmer Lambda 25 spectrometer, at 400 nm, against a calibration curve of KH_2PO_4 standard solutions.

The total iron concentration was determined by an Inductively Coupled Plasma (ICP) optical emission spectrometer (Optima 7000 DV, Perkin Elmer, USA) with radial configuration. The concentration of Fe (III), on the other hand, was determined with a spectrophotometric method, by measuring the absorbance of the complex formed between the Fe (III) and thiocyanate SCN^- ions at 447 nm,[20] against a calibration curve of Fe (III) standard solutions. Fe (II) concentration was determined by subtracting the Fe (III) concentration from the total iron concentration.

The phase composition of the samples was determined using X-ray diffraction (XRD). Semi-quantitative phase analysis (QPA), which estimates the relative amounts of crystalline phases in the

samples without accounting for any amorphous phase present, was made using the Rietveld method. XRD data for QPA were collected using a θ/θ diffractometer (PANalytical X'Pert Pro, NL) equipped with a fast RTMS detector (PANalytical PIXcel-1D) with Cu Kα radiation (40kV and 40 mA, 20-80 °2θ range, a virtual step scan of 0.02 °2θ, and virtual time per step of 50 s). Instrumental contribution, obtained from the NIST SRM 660b standard (LaB$_6$), was also taken into account in the refinement. The starting atomic parameters for HAp, Ca$_9$FeH(PO$_4$)$_7$ and α-Fe$_2$O$_3$ were taken from the literature.[21-23] The Rietveld data analysis was then performed using the GSAS software package, taking advantage of its graphical interface EXPGUI.[24-25] The following parameters were refined: scale-factors, zero-point, six coefficients of the shifted Chebyshev function to fit the background, unit cell parameters, and two Lorentzian (L_X and L_Y) terms for profile coefficients.

FT-IR spectroscopy was performed with a Perkin Elmer Spectrum 100. To acquire the spectra, about 5 mg of sample was mixed with 200 mg of KBr; the homogeneous mixture was then pressed into a pellet. Spectra were acquired in transmittance mode.

Sample surface morphology was analysed with Scanning Electron Microscopy (SEM), using a Hitachi S-4100 at 25 kV. Because of its insulating properties, the powder was pressed into discs and then sputtered with a gold/platinum coating before the analysis.

UV-vis spectra were taken using a Shimadzu UV 3100 spectrometer equipped with an integrating sphere, covering a wavelength range between 250 and 850 nm (0.2 nm step-size, BaSO$_4$ as reference). UV-vis spectra were taken of the fish bone derived powder, as well as for commercial samples of TiO$_2$ and ZnO (P25 Degussa and Merck, respectively).

Powder photoactivity

To test the photoactivity of the powder, a test with 2,2'-azino-bis-3-ethylbenzthiazoline-6sulphonic acid (ABTS) was used. ABTS was dissolved in water and appropriately diluted to have an absorbance value of about 0.720 for λ = 734 nm. A powder sample solution, with a concentration of 1.0 mg/ml, was prepared; appropriate aliquots of the solution were added to the ABTS solution in a closed 5 cm petri dish; the final concentration of the powder was 0.125 mg/ml, while the total volume was 5 ml. The dishes were then irradiated with both UV and white light. For the UV irradiation, a XX-15 BLB UVP lamp was used (λ_{max} = 365 nm), with an irradiation density of 0.80 mW cm^{-2}. For the white light, a Philips TLD 58W/84 fluorescent lamp, with spectral emission of 400 nm < λ < 700 nm was employed. In both cases, the irradiation time was 15 minutes.

At the end of the irradiation, samples were centrifuged at 7000 rpm for 10 minutes, to separate the powder from the solution. The absorbance of the supernatant was then measured at λ = 734 nm.

The test was performed for the powder derived from fish bones, as well as for commercial TiO$_2$ and ZnO powders (see above). Control experiments were performed with samples kept in the dark for the same interval of time.

Cream preparation

The cream used to incorporate the powder was an emulsion made of two phases, one aqueous and one oily. The oily phase was made of Tegocare 450 ® with capric, stearic and cetylic acids, in concentrations of 3, 4, 2 and 3 w/w respectively; the water phase, on the other hand, was made of glycerine and xantham gum in concentrations of 2 and 0.6 w/w. The final weight was then adjusted to 100 g with the addition of distilled water. The two phases were prepared separately, heated at 80-90 °C and then mixed when they were still warm.

The powder was added to the emulsion in different concentrations – between 1 and 20%. Two sets of experiments were carried out: in the first the powder was added when the emulsion was still hot, while in the second the powder was added when the emulsion had been cooled down to room temperature. These two kinds of experiments correspond to the emulsions **H** and **C** respectively. As a reference (**R**), a cream with no additive, was also prepared. For both sets of experiments, the emulsion was stirred using a R17 Marienfeld mechanical stirrer while the powder was added. The stirring rate was different depending on the amount of powder added; in all cases, however, care was taken to ensure a homogeneous distribution of the powder in the emulsion.

Cream testing

Cream colour

The colour of the creams was measured using a Konica Minolta Spectrometer CM-700d); the instrument was calibrated with a standard white plate, with coordinates L = 97.59, a* = 0.07, b* = 1.89. Data were expressed using the CIELab system. For each cream, the difference in colour was evaluated with the formula:

$$\Delta E = [(L_{sample} - L_{reference})^2 + (a^*_{sample} - a^*_{reference})^2 + (b^*_{sample} - b^*_{reference})^2]^{0.5}$$

where the reference is the cream without the addition of any powder (**R**).

Statistical analysis (Anova test) was performed to compare the colour data, with a 95 % probability (P < 0.05).

In vitro determination of UV protection

The photoprotection efficiency of the creams was determined by measuring the UV-Vis absorption spectra, with the same spectrometer used for the powder sample (see above). For the measurements, a weighed amount of cream was uniformly spread on the base of a polystyrene petri dish, forming a 2 mm thick layer. Prior to the testing, the cream was dried at 45 °C for 1 hour. Two measurements were taken for each sample. The UV-Vis spectrum of the polystyrene plate was also acquired, and subtracted from the spectra of each cream sample.

The effectiveness of the UV protection was evaluated by the critical wavelength method,[26] where the value of the critical wavelength was calculated with the formula:

$$\int_{290}^{\lambda_{crit}} A_\lambda d\lambda = 0.9 * \int_{290}^{400} A_\lambda d\lambda$$

Moreover, the UVA/UVB ratio was also calculated,[27] according to the formula:

$$R = \frac{\int_{320}^{400} \frac{A_\lambda d\lambda}{\int_{320}^{400} d\lambda}}{\int_{290}^{320} \frac{A_\lambda d\lambda}{\int_{290}^{320} d\lambda}}$$

Cream photostability

To establish the stability of the creams, and their efficacy as photoprotectors, all samples were irradiated with both UV and white light, using the same light sources described above. The irradiation times were 3 and 1 hour for UV and white light respectively. After the irradiation, the UV-Vis spectra of all samples were acquired again.

The stability was assessed with the Area Under the Curve Index (AUCI); according to literature,[28] the AUCI parameter is calculated considering the area under the curve (AUC) of the UV absorption spectrum in the interval 290 – 400 nm. This area is calculated before and after the irradiation, with the AUCI being: AUCI = (AUC)$_{after}$/(AUC)$_{before}$. If the AUCI is higher than 0.8, the sunscreen is considered stable. The same calculation was done considering the intervals 320 – 400 and 290 – 320 nm to determine the specific stability in the UVA and UVB regions (AUCI$_A$ and AUCI$_B$, respectively).

In vivo test of the acute irritant potential

To assess the safety of the developed cosmetic product, its acute irritant potential was tested in human volunteers after a single application under occlusion (patch test). The effect of the selected samples of cream on human skin was tested according to Colipa protocol,[29] on 20 healthy volunteers; their group age was 20 – 50, subjects with previous problems of skin sensitivity and skin allergic reactions were excluded. Finn Chambers on Scanpor (8 mm diameter, SmartPractice ®) were used to put the cream in contact with the skin. About half of the volume of each chamber was carefully filled with the cream; then a patch was applied to the forearm of the volunteer. As a negative control, the cream without any additive (**R**) was also used. After 48 hours, the patches were removed and the reaction of the skin was evaluated 30 minutes after the patch removal, following the ESCD guidelines. The guidelines are based on a scoring scale from 0 to 4, where 0 corresponds to no skin reaction/irritation while 4 indicates a very strong reaction.[30] This study was performed following the WMA Declaration of Helsinki and the Informed Consent protocol.

Results and discussion

Materials characterisation

Figure 1 shows the XRD diffraction pattern for the powder obtained after Fe (II) solution treatment and calcination of the fish bones (sample **HAp-Fe**); the corresponding phase composition is reported Table 1. It can be seen that, although HAp is still present, it
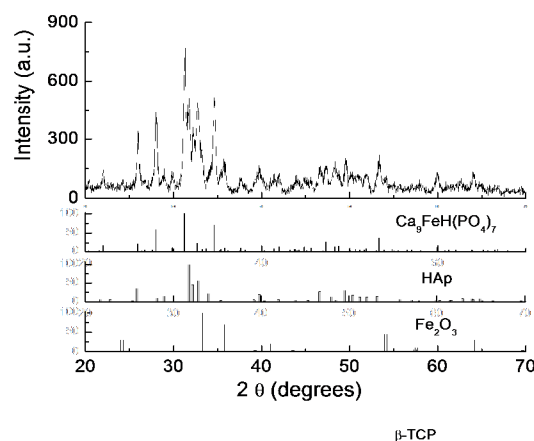

Figure 1. XRD pattern for sample **Fe-HAp**.

Table 1. Phase and elemental composition of **HAp-Fe** sample; all values are expressed as weight %. For the phase analysis, Rietveld agreement factors were: R_{wp} = 5.90%, $R_{(F^2)}$ = 6.04%, χ^2 = 1.63.

Phase	Concentration
$Ca_{10}(PO_4)_6(OH)_2$	42.9(3)
α-Fe_2O_3	2.0(2)
$Ca_9FeH(PO_4)_7$	55.0(3)
Element	
Ca	31.64
P	18.59
Fe total	3.90
Fe (III)	1.04
Fe (II)	2.86

is not the main phase anymore, as its concentration is about 43 wt %. The main component is a different phosphate-based compound, which contains both iron and calcium – $Ca_9FeH(PO_4)_7$ (calcium hydrogen iron phosphate), with about 55 wt% concentration. Further to this, a small amount of 2 wt% hematite was also detected, at the limits of XRD sensitivity – the actual amount may well be less than 2 wt%. The detection of these phases indicates that iron is present with two different oxidation states, both as Fe (II) and Fe (III), in the mixed phosphate and hematite, respectively.

To explain this, the chemical reactions taking place in solution and during the calcination have to be considered. In solution, the addition of a base led to the formation of Fe (II) oxide, which formed a suspension; the colour change of the solution from green to dark brown/black confirmed this. When the bones were treated in solution, some of the Fe (II) was substituted into the HAp lattice, due to an ion exchange process. Indeed, it is well known that the HAp lattice structure favours the exchange between Ca (II) and other divalent ions.[31] Moreover, in this case the ion exchange is also favoured by the porous structure of the bones themselves. During the calcination, Fe-containing HAp was partially converted into Fe-containing phosphate, leading to the formation of $Ca_9FeH(PO_4)_7$; this process was previously reported in literature for HAp samples with iron embedded into their lattice.[32]

Further to the ion exchange, however, the Fe (II) oxide suspension also formed a layer on the surface of the bones; this could be observed, as at the end of the treatment the bones had a darker colour. During the calcination, an oxidation of this iron oxide took place, due to the reaction of Fe (II) with atmospheric oxygen, resulting in the formation of Fe (III) oxide in the form of hematite.

Table 1 also shows the elemental analysis of the powder. The data confirm the presence of iron in both forms; in fact it can be seen that the total iron concentration is higher than the Fe (III) concentration alone (Fe(III) ~27% of total Fe), indicating the presence of Fe (II) as well. These data are in agreement, within the experimental error, with the phase composition values calculated by XRD semi-quantitative phase analysis.

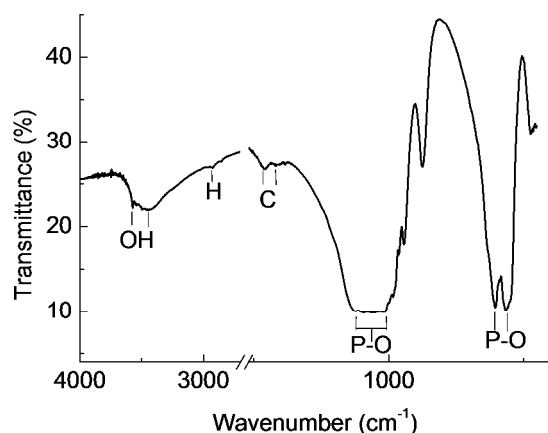Figure 3. SEM micrography for sample **Fe-HAp**, 50 000 magnifications.

Figure 2. Infrared spectrum of the sample **Fe-HAp**.

In Figure 2, the IR spectrum of sample **HAp-Fe** is reported. The P-O related peaks can be observed in wavelength intervals of $540 - 620$ cm^{-1} and $900 - 1200$ cm^{-1}. Considering this last region in particular, it can be seen that the spectrum just shows one broad peak, and not several sharp ones as is normally observed for HAp.[33] This behaviour was previously reported for $Ca_9FeH(PO_4)_7$;[23] it therefore confirms the presence of this phase in the material. The small peak detected at 2925 cm^{-1} also belongs to $Ca_9FeH(PO_4)_7$, as it is due to the proton present in this molecule.[23]

The spectrum also has signals in the 1410-1460 cm^{-1} region, which correspond to carbonate ions; their presence is due to the fact that organic fragments may still be present in the powder. In fact, literature reports that a complete elimination of the organic fraction from the bones can take place only for temperatures as high as 1000 °C.[34] The broad signal at 3450 cm^{-1}, together with the small sharp peak at 3570 cm^{-1}, is due to the OH group of the HAp molecule.[18]

Figure 3 shows the SEM micrography of **HAp-Fe** powder. It can be seen that the material consists of small, submicron, irregularly-shaped grains, with diameters between ~50-200 nm. Most of the particles appear to be around 100 nm, making this a borderline nanomaterial, and they appear to be poorly crystalline in nature, reflecting the relatively broad and noisy XRD pattern obtained. This is reasonable considering the relatively low calcination temperature (700 °C).
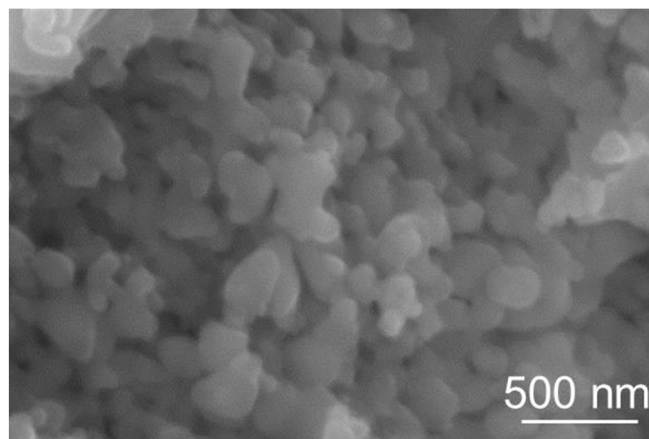
Figure 4(a) reports the UV-Vis spectrum of **HAp-Fe**, shown in absorbance mode; the sample absorbs both in the UVA and UVB regions, showing great potential as a sunscreen. In the spectrum, two broad peaks can be observed, centred at about 300 and 408 nm respectively; a shoulder at about 526 nm is also present.

The characteristics observed in the spectra are in agreement with literature data for α-Fe_2O_3, as in the Fe (III) oxide spectrum the most intense UV absorption bands correspond to 290 and 395 nm. They are ascribed to the metal-ligand charge transfer (MLCT), and to a certain extent, also to contribution of Fe^{3+} ligand field transitions: $^6A_1 \rightarrow {}^4T_1(^4P)$ at 290-310 nm, and $^6A^1 \rightarrow {}^4E(^4D)$ and $^6A_1 \rightarrow {}^4T_2(^4D)$ at 360-400 nm.[35,36] The exact position of these bands, however, can vary due to the characteristics of the powder; in the case of nanoparticles, for instance, the diameter of the particle can affect the light absorption.[37,38] A similar effect was observed for nanorods, where the values of both diameter and length of the rods influenced the position of the absorption maximum and the intensity of the absorption.[39] Analogously, the absorption in the visible region, and hence the colour of the powder, can also depend on the crystallite size.[13]

The presence of a peak at about 290 – 300 nm was also observed for iron-substituted HAp;[40,41] these data are, therefore, in agreement with the hypothesis of iron incorporation into the HAp lattice. This would also explain why we have such a strong absorbance throughout the UVA and UVB regions – above 60% from 290-400 nm – with such a small amount (no more than 2 wt%) of hematite. The $Ca_9FeH(PO_4)_7$ phase (55 wt%) must also be contributing significantly to the absorption of UV radiation.

Figure 4(b) shows the normalised absorption of samples **Fe-HAp** and commercial TiO_2 and ZnO powders; these measurements were performed to compare the UV absorption range of **Fe-HAp** to that of powders already used for sunscreens. It can be seen that Fe-HAp absorbs for the whole UV range, whereas both commercial samples do not show this feature; in fact their absorption starts to decrease at about 315 and 350 nm for TiO_2 and ZnO, respectively. The larger UV absorption range shows that, potentially, **Fe-HAp** could be a sunscreen with better performance in the UVA interval than some of the commercial samples.
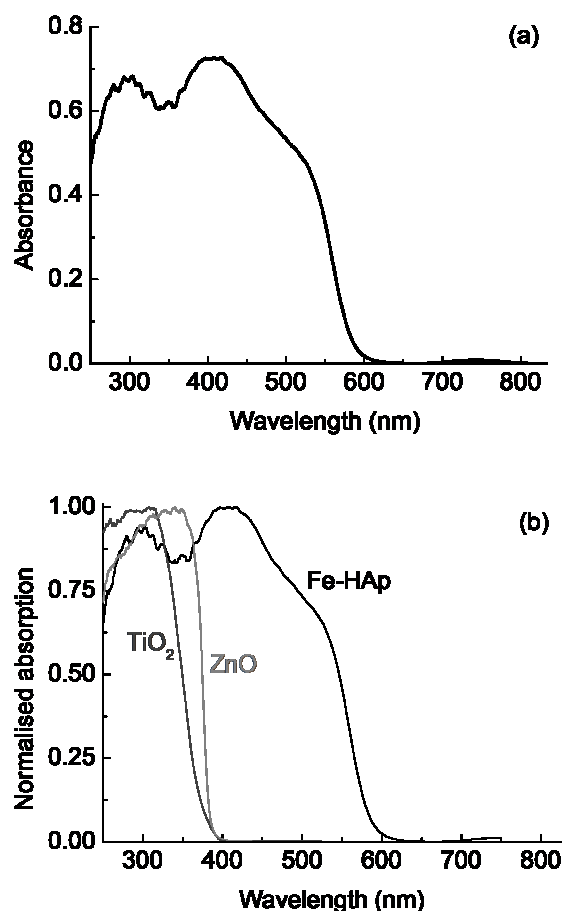
clear decrease can be seen. Under white light, there is a slight decrease in the absorption value; the difference, however, is not statistically significant (P < 0.05). In any case, the change observed is smaller than that registered for both TiO_2 and ZnO. These data indicate that Fe-HAp is less photoreactive than other inorganic materials used as sunscreen filters; hence, it potentially represents a safer option for a cream formulation.

Figure 4. (a) UV spectrum of the sample **Fe-HAp** in absorbance mode. (b) Normalised absorption for samples **Fe-HAp** (black), commercial TiO_2 P25 (dark gray) and commercial ZnO Merck (gray).
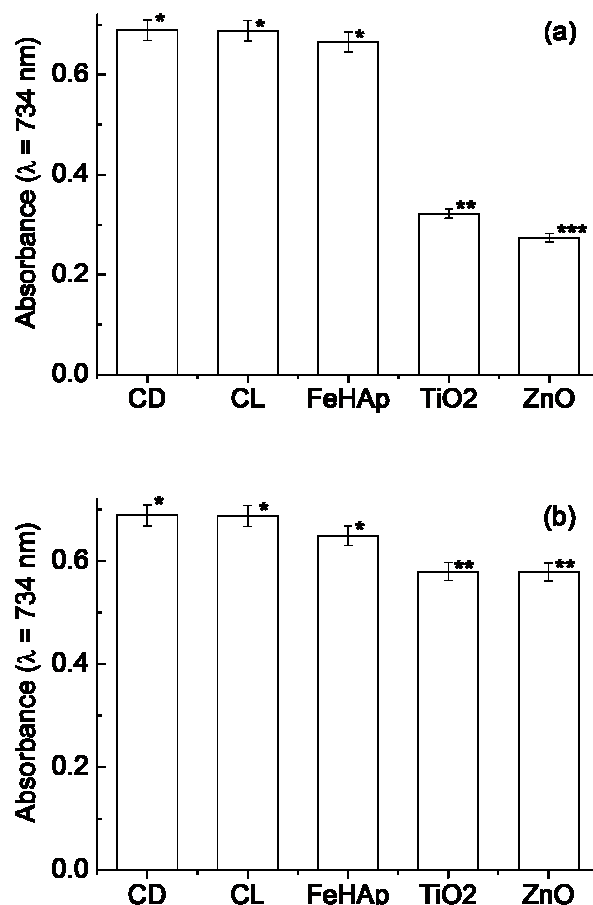
Figure 5. Absorbance of ABTS radical under (a) UV and (b) white light irradiation. CD: control sample in the dark; CL: ABTS solution under light irradiation without any powder; Fe-HAp, TiO2 and ZnO: ABTS under light irradiation in contact with powder samples **Fe-HAp**, commercial TiO_2 P25 and commercial ZnO Merck respectively. Column with the same symbol (*, ** or ***) indicate that data are NOT statistically different.

Testing of the powder photoactivity

To test the potential of **Fe-Hap** sample as an inert sunscreen material, its photoactivity was tested under both UV and white light. A protocol similar to that reported in literature was used.[42] The powder was irradiated and, to see if any radical/reactive species were formed, the subsequent reaction with a radical such as ABTS was measured. ABTS was chosen as reagent due to its greater sensitivity if compared with other reagents such as DPPH;[43] moreover, it was previously used to monitor the photoactivity of materials such as TiO_2.[44] The extent of the reaction was monitored by measuring the absorbance at λ = 734 nm. With no radical formation, no reaction should take place and, hence, no change in colour should be observed; the formation of radicals, on the other hand, should lead to a color change in the ABTS solution.

For comparison purposes, the test was also performed for commercial TiO_2 and ZnO; the results are shown in Figure 5(a) and 5(b) for UV and white light irradiation, respectively. It can be seen that, under UV light, there is no change in the ABTS absorption for Fe-HAp containing solution; for TiO_2 and ZnO, on the other hand, a

Testing of the cream: UV protection and photostability

Table 2 reports the composition of the emulsions prepared adding the **HAp-Fe** powder to the basic emulsion (see "Cream preparation" section). It can be seen that different powder quantities were added, to see how the additive concentration could affect the absorbing properties of the cream. A maximum **HAp-Fe** content of 20 wt% was chosen, considering the maximum concentration normally used for other inorganic sunscreens.[5]

Table 2. Emulsions prepared adding different amounts of **HAp-Fe** sample. The letters H and C indicates that the powder was added to the hot or cold emulsions respectively.

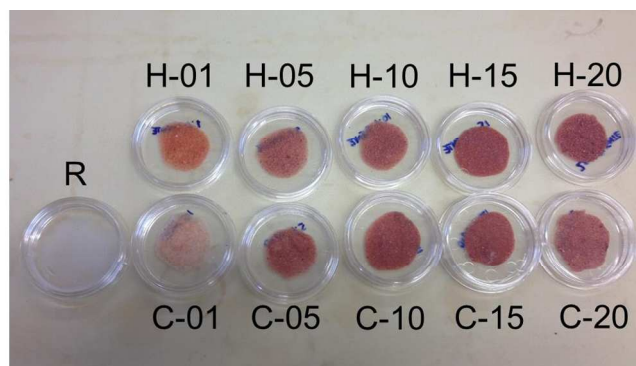| Sample name	Powder concentration (% w/w)
R	0
H-01	1
H-05	5
H-10	10
H-15	15
H-20	20
C-01	1
C-05	5
C-10	10
C-15	15
C-20	20

Figure 6. Picture of the creams prepared, as detailed in Table 2.

Table 3. CIELab coordinates for the cream samples.

Sample	L	a*	b*	□E
R	55.32 ± 0.56 [a]	-0.40 ± 0.03 [a]	1.47 ± 1.19 [a]	-
H-01	30.21 ± 0.72 [b]	11.18 ± 0.43 [b]	10.70 ± 0.17 [b]	29.15 ± 0.65 [a]
H-05	27.25 ± 0.91 [c]	10.30 ± 0.46 [b]	8.08 ± 0.20 [c]	30.76 ± 0.79 [a]
H-10	24.29 ± 0.83 [d]	10.67 ± 0.08 [b]	7.33 ± 0.37 [d]	33.46 ± 0.59 [b]
H-15	23.51 ± 0.17 [d]	11.28 ± 0.31 [b]	6.99 ± 0.19 [d]	34.33 ± 0.64 [b]
H-20	23.98 ± 0.43 [d]	10.15 ± 0.31 [b]	6.18 ± 0.16 [e]	33.40 ± 0.62 [b]
C-01	39.43 ± 0.73 [e]	5.62 ± 0.54 [c]	8.09 ± 0.36 [c]	18.23 ± 0.84 [c]
C-05	27.79 ± 0.58 [c]	9.85 ± 0.37 [b]	8.17 ± 0.60 [c]	30.13 ± 0.77 [a]
C-10	25.75 ± 0.36 [f]	11.13 ± 0.05 [b]	7.60 ± 0.11 [d]	32.32 ± 0.61 [b]
C-15	25.16 ± 0.26 [f]	11.21 ± 0.24 [b]	7.42 ± 0.19 [d]	32.86 ± 0.63 [b]
C-20	27.44 ± 0.15 [c]	10.12 ± 0.29 [b]	7.13 ± 0.17 [d]	30.33 ± 0.69 [a]

Note: different letters in the same column indicate that data are statistically different (P<0.05).

Figure 6 shows a picture of all the creams with different powder concentrations, as well as the reference cream. It can be seen how the cream colour changes depending on the additive content and the preparation method. The pictures show that all creams have a colour which is similar to other cosmetic products, and for that, acceptable for the consumer.

To evaluate quantitatively the colour of each cream, the CIELab coordinate system was used; the results for each cream are listed in Table 3, together with the total difference in colour ΔE. A statistical analysis was also performed to compare the same parameter (CIELab coordinate or ΔE) for different creams (i.e. a comparison of the different data in the same table column).

In the creams prepared at high temperature (samples **H**), a decrease in the luminosity parameter L is observed in comparison to the reference cream **R**; such decrease is more marked for the creams with higher **HAp-Fe** powder concentrations. Both a* and b* values, on the other hand, are higher than for the unmodified emulsion **R**, indicating a colour shift towards the red and the yellow respectively. For the a* parameter, however, there is no statistical difference between the various samples, while for b* a significant (P<0.05)

decrease with increasing additive concentration can be observed. Those prepared in cold conditions (samples **C**) also present a decrease in the L value, but they exhibit a clear general increase in a*, along with a much smaller general decrease in b*, with increasing **HAp-Fe** content. Apart from sample **C01**, all cream samples with **HAp-Fe** powder added exhibited similar colour change (ΔE) values of 29-34. Considering the difference in ΔE between creams prepared under hot and cold conditions, samples with 5, 10 and 15 wt% additive contents showed comparable ΔE values (values not statistically different, P>0.05), regardless of the preparation conditions. The creams with 1 and 20 wt% additive concentrations, however, did not follow this pattern; in fact those prepared in cold conditions (**C01** and **C20**) had lower ΔE values than those prepared warm (**H01** and **H20**). This may be because in the creams prepared at higher temperatures, a more homogenous mixture between the powder and the emulsion was obtained; the effect that the powder has on the colour is, therefore, more enhanced.

The UV-Vis spectra of the creams prepared in hot and cold conditions are shown in Figure 7(a) and 7(b) respectively; the spectrum of the unmodified cream (**R**) is also shown in both graphs. It can be seen that **R** shows very little absorption in the UV and
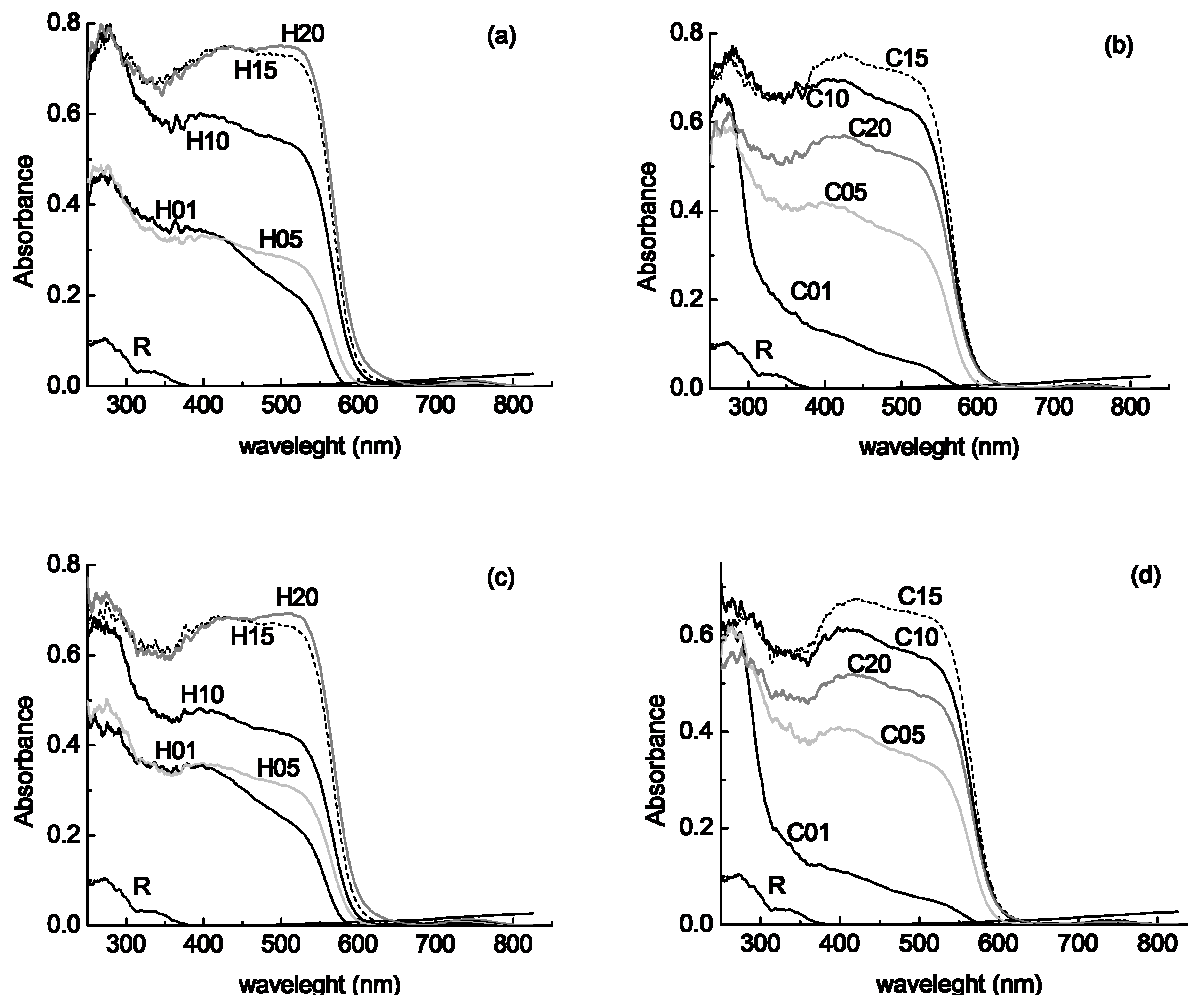
Journal Name

ARTICLE

Figure 7. UV spectra for the cream samples; (a-b) spectra of the creams as prepared; (c-d) spectra of the creams after light irradiation; (a-c) creams prepared with hot emulsion; (b-d) creams prepared with cold emulsion.

almost none in the visible; this later was predictable from its white colour (see Figure 6 and Table 3). Considering Figure 7(a), it can be seen that the absorption spectrum of all creams maintained the same profile of the powder, as shown in Figure 4(a), with absorption over the whole UV range. Spectra of samples **H01** and **H05** show almost no difference; a further increase in the additive concentration led to an increase in the value of the absorption, as can be seen for samples **H10** and **H15**. A **HAp-Fe** content higher than 15%, however, did not cause any further increase in the UV absorption; in fact the spectra of sample **H15** and **H20** are practically identical (within experimental error).

The samples prepared at room temperature, on the other hand, show different characteristics. Sample **C01**, in particular, shows high absorption only for wavelengths smaller than 300 nm; for higher values a sudden decrease can be observed. Creams with higher additive content have a similar absorption profile to the **HAp-Fe** powder; it is interesting to note, however, that sample **C20** has a lower absorption than **C10** and **C15**. Both these anomalies could be due to an incomplete homogenisation and distribution of the additive in the cream paste due to the lower temperature. For **C01**, it is possible that, as the powder was not well distributed and in lower concentration, its contribution to the absorption could have been smaller. For sample **C20**, on the other hand, **HAp-Fe** content may

have been too high in the cream to embed itself into the structure of the cream properly with the mixing performed at room temperature. The subsequent lack of homogenisation may have had a significant effect on the UV-Vis properties.

To evaluate the effectiveness of the protective action, the critical wavelength λ_{crit} and the UVA/UVB ratio were calculated; they are shown in Table 4. It can be seen that the majority of samples have a λ_{crit} value between 388 and 390 nm; the only exception is **C01**, with a value of 382 nm, as its absorption in the UVA range is lower due to the reasons aforementioned. However, all λ_{crit} values are higher than 370 nm; therefore, all creams can all be classified as broad spectrum sunscreen.[27] These λ_{crit} values are comparable with those of other commercially available inorganic sunscreens.[1]

Table 4. Critical wavelength λ_{crit} and UVA/UVB ratio for the cream samples.

Sample	λ_{crit} (nm)	UVA/UVB ratio
H-01	388 – 389	0.983
H-05	388 – 389	0.942
H-10	388 – 389	0.920
H-15	389 – 390	1.029
H-20	389 – 390	1.025
C-01	382 – 383	0.570
C-05	388 – 389	0.938
C-10	389 – 390	1.017
C-15	389 – 390	1.066
C-20	389 – 390	1.044

Moreover, almost every cream has a UVA/UVB ratio higher than 0.90 (Table 4) - again the exception is sample **C01** (UVA/UVB = 0.570) - for the absorption characteristics described above. In particular, samples **H15**, **H20**, **C10**, **C15** and **C20** have values very close to 1; this means they can offer an effective comparable protection over the UVA range as well as UVB. Using the *Boots Star Rating* classification system, developed by Boots, one of the UK's main sunscreen producers and retailers, these creams would be rated as 5 stars, offering the maximum UVA protection.[45]

Although these tests were not performed following exactly the COLIPA protocol, data reported here already give a very clear indication about the effectiveness of these creams as sunscreens. In fact, literature data shows that parameters such as the critical wavelength and the UVA/UVB ratio are weakly affected by experimental conditions, such as the nature of the substrate and the thickness of the cream layer used in the UV spectra measurements.[28]

To test the photostability of the creams, they were irradiated and then assessed again, as described in the experimental section; the acquired UV spectra are shown in Figures 7(c) and 7(d), respectively. It can be seen that for both sets of samples, there are few changes in their absorption behaviour; in fact in all cases the absorption profile is not affected by the light irradiation. A decrease in the absorption intensity, however, was observed in some of the irradiated samples. The smaller absorption may be due to an increase in the crystallite size induced by the irradiation, and this behaviour

was previously observed and reported.[40] Concerning the stability of the organic components of the emulsion under irradiation, literature data showed their degradation is mainly due to the photoactivity of the inorganic filters such as TiO_2 and ZnO.[46] In this case, however, **Fe-HAp** does not show significant photoactivity; therefore it is reasonable to assume that no degradation takes place.

To quantify the decrease, the AUCI, $AUCI_A$ and $AUCI_B$ ratios were evaluated (see Table 5). In all cases the indexes were higher than 0.80, a value which is normally considered a stability indicator;[28] this was observed for the whole UV range, for the UVA and for the UVB subintervals. Moreover, for all creams the irradiation did not cause any change in the value of the critical wavelength λ_{crit}. These data clearly indicate the photostability of these samples.

Table 5. AUCI, $AUCI_A$ and $AUCI_B$ values for the creams.

Sample	AUCI	$AUCI_A$	$AUCI_B$
H-01	0.986	0.956	0.998
H-05	0.956	0.895	0.999
H-10	0.828	0.823	0.898
H-15	0.914	0.934	0.988
H-20	0.919	0.927	0.999
C-01	0.882	0.900	0.996
C-05	0.984	0.999	0.903
C-10	0.866	0.877	0.935
C-15	0.873	0.898	0.946
C-20	0.919	0.941	0.999

Testing of the cream: acute cutaneous irritation potential

A test of acute irritation potential was performed to check whether these creams can be tolerated by the skin, without the active compounds causing any irritant reaction. The cream considered for the test was **H-15**; this was chosen because of its high absorbance, UVA/UVB ratio and irradiation stability.

Figure 8. Picture of the areas of the skin tested with the creams. R: Finn chamber with reference cream **R**; H-15: Finn chambers with sample **H-15**.

Figure 8 shows a picture of the area of the skin in contact with the cream. It can be seen that no irritation or erythema formation could be detected. Indeed, the part of the skin in contact with sample **H-15** has the same appearance of the part in contact with reference sample **R**. Considering the score system used to evaluate the skin reaction, this corresponded to a 0 score. The same behaviour, and therefore 0 score, was observed for all 20 volunteers tested.

Therefore, it can be concluded that these products are not expected to cause any irritant reaction in healthy people, and that they could be safely used. This result was expected, as none of the components have a toxic nature; in fact HAp is present in large amounts in the human body, is a fully biocompatible material used in bio-implants and bone scaffolds, and Fe_2O_3 is already used as an additive in many cosmetic products. This study proves that also their interaction with cream matrix compounds can be considered safe.

Conclusions

A HAp-based compound, which contains α-Fe_2O_3 in hematite form, was successfully developed from fish cod bones; this was achieved with a simple process of treating the bones in Fe (II) containing solution and successive bones calcination at 700 ^{o}C. The material showed good absorption properties in the UV range, and it does not form radicals and/or reactive species under irradiation; it was, therefore, used in the formulation of a sunscreen cream; this is the first time a HAp-based sunscreen cream was developed.

Tests of the cream containing 15 % of the powder revealed that it could be used as a broad sunscreen protector ($\lambda_{crit} > 370$ nm), as it shows high absorption both in the UVA and UVB ranges; because of its absorption properties it would be classified as 5 stars according to Boots UVA protection categories. The cream is also photostable and it does not cause irritation or erythema formation when in contact with human skin.

These results show how a food by-product such as fish bones could be converted into a valuable product. Future work will be performed to optimise both the material properties and the cream formulation. Further to the potential in cosmetics reported in this study, possible applications in other sectors, such as medicine, will also be considered.

Acknowledgements

Notes

[a] Centro de Biotecnologia e Química Fina – Laboratório Associado, Escola Superior de Biotecnologia, Universidade Católica Portuguesa, Porto, PORTUGAL.

[b] Departmento de Ciencias Biomedicas e Medicina, Universidade do Algarve, Faro, PORTUGAL.

[c] Departemento Engenharia de Materiais e Cerâmica / CICECO, Universidade de Aveiro, Campus Universitário de Santiago, 3810-193, Aveiro, PORTUGAL.

[d] Inovapotek, Pharmaceutical Research and Development, Porto, PORTUGAL.

*: corresponding author, cpiccirillo@porto.ucp.pt

References

1. M.D. Palm, M.N. O'Donoghue, *Dermat. Ther.*, 2007, **20**, 360.
2. N. Serpone, D. Dondi, A. Albini, *Inorg. Chim. Acta*, 2007, **360**, 794.
3. D. Moydal, A.M. Fourtanier, *J. Amer. Acad. Dermat.*, 2008, **58**, S149.
4. D. Moyal, A. Chardon, N. Kollias, *Photoderm. Photoimm. Photomed.*, 2000, **16**, 250.
5. R. Jansen, U. Osterwald, S.Q. Wang, M. Burnett, H.W. Lim, *J. Amer. Acad. Dermat.*, 2013, **69**, 867.
6. P. Singh, A. Nanda, *Int. J. Cosmet. Sci.*, 2014, **36**, 273.
7. E. Gilbert, F. Pirot, V. Bertholle, L. Roussel, F. Falson, K. Padois, *Int. J. Cosmet. Sci.*, 2013, **35**, 208.
8. T.G. Smijs, S. Pavel, *Nanotech, Sci. Appl.*, 2011, **4**, 95.
9. Z.A.M. Lewicka, W.W. Yu, B.L. Oliva, E.Q. Contreras, V.L. Colvin, *J. Photoch. Photobiol. A Chem.*, 2013, **263**, 24.
10. P. Tucci, G. Porta, M. Agostini, D. Dinsdale, I. Iavicoli, K. Cain, A. Finazzi-Agro, G. Melino, A. Willis, *Cell Death Disease*, 2013, **4**, e549.
11. A. Tovar-Sánchez, D. Sánchez-Quiles, G. Basterretxea, J.L. Benedé, A. Chisvert, A. Salvador, I. Moreno-Garrido, J. Blasco, *PLoS ONE*, 2013, doi:10.1371/journal.pone.0065451.g001.
12. N.C. Dlova, F.T. Nevondo, E.M. Mwangi, B. Summers, J. Tsoka-Gwegweni, B.C. Martincigh, D.A. Mulholland, *Photoderm. Photoimm. Photomed.*, 2013, **29**, 164.
13. L. Truffault, B. Choquenet, K. Kostantinov, T. Devers, C. Couteau, L.J.M. Coiffard, *J. Nanosci. Nanotech.*, 2010, **10**, 1.
14. S.V. Dorozhkin, *Biomater.*, 2010, **31**, 1465.
15. T.S. de Araujo, S.O. de Souza, E.M.B. de Souza, *J. Phys. Confer. Series*, 2010, **249**, 012012.
16. T.S. de Araujo, S.O. de Souza, W. Miyakawa, E.M.B. de Souza, *Mater. Chem. Phys.*, 2010, **124**, 1071.
17. D. Holzmann, D. Holzinger, G. Hesser, T. Schmidt, G. Knör, *J. Mater. Chem.*, 2009, **19**, 8102.
18. C. Piccirillo, M.F. Silva, R.C. Pullar, I. Braga da Cruz, R. Jorge, M.M.E. Pintado, P.M.L Castro, *Mat. Sci. Eng. C*, 2013, **33**, 103.
19. C. Piccirillo, C.W. Dunnill, R.C. Pullar, D.M. Tobaldi, J.A. Labrincha I.P Parkin, *J. Mat. Chem. A*, 2013, **1**, 6452.
20. C.R. Clark, *J. Chem. Educ.*, 1997, **74**, 1214.
21. C. Piccirillo R.A. Pinto D.M. Tobaldi R.C. Pullar, J.A. Labrincha, M.M.E. Pintado, P.M.L Castro, Submitted.
22. B.I. Lazoryak, V.A. Morozov, A.A. Belik, S.S. Khasanov, V.S. Shekhtman, *J. Sol. State Chem.*, 1996, **122**, 15.
23. M. Dondi, F. Matteucci, G. Cruciani, G. Gasparotto, D.M. Tobaldi, *Solid State Sci*, 2007, **9** 362.
24. A.C. Larson, R.B. Von Dreele, General Structure Analysis System (GSAS). *Los Alamos National Laboratory Report LAUR*, 2004.
25. B.H. Toby, *J. Appl. Cryst.*, 2001, **34**, 210.

26. Colipa, *In vitro* method for the determination of the UVA protection factor and "critical wavelength" values of sunscreen products. Revised Guidelines (2011).

27. M.V.R. Velasco, F.D. Sarruf, I.M.N. Salgado-Santos, C.A. Haroutionian-Filho, T.M. Kaneko, A.R. Baby, *Int. J. Pharmac.*, 2008, **363**, 50.

28. D. Garoli, M.G. Pelizzo, B. Bernardini, P. Nicolosi, M. Alaibac, *J. Dermat. Sci.*, 2008, **52**, 193.

29. Colipa, Assessment of skin tolerance of potentially irritant cosmetic ingredients. Guidelines (2007).

30. R.A. Tupker, C. Willis, E. Berardesca, C.H. Lee, M. Fartasch, T. Agner, J. Serup, *Cont. Derm.*, 1997, **37**, 53.

31. A. Nzihou, P. Sharrock, *Waste Biom. Valor.*, 2012, **1**, 163.

32. A. Tampieri, T. D'Alessandro, M. Sandri, S. Sprio, E. Landi, L. Bertinetti, S. Panseri, G. Pepponi, J. Geottlicher, M. Bañobre-López, J. Rivas, *Acta Biomat.*, 2012, **8**, 843.

33. K. Haberko, M.M. Bucko, J. Brzezinska-Miecznik, M. Haberko, W. Mozgawa, T. Panz, A. Pyda, J. Zarebski, *J. Europ. Ceram. Soc.*, 2006, **26**, 537.

34. M. Figueiredo, A. Fernando, G. Martins, J. Freitas, F. Judas, H. Figueiredo, *Ceram. Intern.*, 2010, **36**, 3283.

35. D.M. Sherman, T.D. Waite, *Amer. Miner.*, 1985, **70**, 1262.

36. Y.P. He, Y.M. Miao, C.R. Li, S.Q. Wang, L. Cao, S.S. Xie, G.Z. Yang, B.S. Zou, *Phys. Rev. B*, 2005, **71**, 125411.

37. J. Lian, X. Duan, J. Ma, P. Peng, T. Kim, W. Zheng, *ACS Nano*, 2009, **3**, 3749.

38. M. Mohammadikish, *Ceram. Intern.*, 2014, **40**, 1351.

39. S. Zeng, K. Tang, T. Li, *J. Coll. Interf. Sci.*, 2007, **312**, 513.

40. Y. Wang, W. Du, Y. Xu, *Langm.*, 2009, **25**, 2895.

41. M. Khachani, M. Kacimi, A. Ensuque, J.Y. Piquemal, C. Connan, F. Bozon-Verduraz, M. Ziyad, *Appl. Catal. A Gen.*, 2010, **388**, 113.

42. L. Tiano, T. Armeni, E. Venditti, G. Barucca, L. Mincarelli, E. Damiani, *Free Rad. Biol. Medic.*, 2010, **49**, 408.

43. A. Floegel, D. Kim, S. Chung, S.I. Koo, O.K. Chun, *J. Food Compos. Anal.*, 2011, **24**, 1043.

44. V. Brezová, Z. Vrecková, P. Billick, M. Čaplovičová, G. Plesch, *J. Photoch. Photobiol. A*, 2009, **206**, 177.

45. A. Springsteen, R. Yurek, M. Frazier, K.F. Carr, *Anal. Chim. Acta*, 1999, **380**, 155.

46. J. Kockler, M. Oelgemöller, S. Robertson, B.D. Glass, *J. Photoch. Photobiol. C*, 2012, **13**, 91.

Hydroxyapatite-Fe$_2$O$_3$ based material of natural origin as an active sunscreen filter

C. Piccirillo, C. Rocha, D.M. Tobaldi, R.C. Pullar, J.A. Labrincha, M.O. Ferreira, P.M.L. Castro, M.M. Pintado.

Hydroxyapatite-Fe$_2$O$_3$ based material of marine origin – fish bones treated in Fe(II)-containing solution – shows potentials as sunscreen filter, absorbing in UVA/UVB intervals, with no free radical formation under irradiation.